AIAA JOURNAL
Vol. 32, No. 2, February 1994

Infrared Imaging of Large-Amplitude, Low-Frequency Disturbances on a Planar Jet

Robert B. Farrington* and Scott D. Claunch†
National Renewable Energy Laboratory, Golden, Colorado 80401

The purpose of this study is to demonstrate that periodic, large-amplitude, low-frequency disturbances on a planar jet can increase spreading and mixing of a planar jet with the surrounding fluid. This is achieved by enhancing the natural instabilities of the jet, resulting in the formation of large vortical structures in the mixing layers. The jet had a Reynolds number of about 7.2×10^3, an aspect ratio of 47, and Strouhal numbers, based on the nozzle width and the disturbance frequency, up to 0.324. A relatively new technique, full-field infrared imaging, was used to determine jet behavior and mixing. This technique provides a significant advantage over conventional temperature measurement techniques. Over 68,000 data points can be monitored as often as 30 times each second. Contour plots of the isotherms of the infrared images showed that the disturbances increased the spread rate of the jet and accelerated the transition of the planar jet into an axisymmetric regime. A relative mixing efficiency was defined and measured. The mixing that occurred within the thermal half-width of the jet when pulsed at $Str = 0.168$ was about 32% greater at seven nozzle widths than that of the natural jet.

Nomenclature

B = nozzle width, m
f = frequency, Hz
L = nozzle length, m
Re = Reynolds number, $u_0 B/\nu$
Str = Strouhal number, fB/u_0
T = temperature, °C
$T_{ambient}$ = room air temperature, °C
T_{jet} = outlet temperature of jet, °C
$T_{max}(X)$ = maximum temperature at axial distance X, °C
$T_{min}(X)$ = minimum temperature at axial distance X, °C
u_0 = exit velocity, $(X, Y, Z) = (0, 0, 0)$, m/s
X = nondimensional axial position, x/B
X_0 = virtual origin of the jet
Y = nondimensional transverse position, y/B
Y^- = left edge of jet
Y^+ = right edge of jet
$Y_{0.5,\,T}$ = thermal half-width
Z = nondimensional longitudinal position, z/L
$\eta(X)$ = thermal mixing efficiency at X
$\eta_r(X)$ = relative mixing efficiency at X
$\Theta(X,Y)$ = nondimensional temperature, $[T(X, Y) - T_{jet}]/[T_{ambient} - T_{jet}]$
$\Theta_{edge}(X)$ = particular value of $[T(X, Y) - T_{min}(X)]/[T_{max}(X) - T_{min}(X)]$
$\Theta_{min}(X)$ = minimum nondimensional temperature at axial distance X
ν = kinematic viscosity, m^2/s

Introduction

INDOOR air quality and thermal comfort in buildings is a result not only of the turnover rate and the temperature of the conditioned air being supplied to occupied areas but also of the efficiency with which the conditioned air mixes with the ambient air. If the ventilation jet produced by a diffuser does not mix thoroughly with the surrounding air, then the conditioned air can short-circuit back to the return air intake, leaving pockets of stagnant air in the room. In these pockets, sometimes called dead zones, thermal comfort is not maintained, and pollutants are not removed, creating a potentially uncomfortable, unhealthy, and unproductive environment.

Slot diffusers, which are commonly found in office spaces, produce a planar jet. Planar geometries are sometimes used, instead of circular diffusers, because of geometries of the occupied space and architectural considerations. This paper discusses the effect of large-amplitude, low-frequency periodic disturbances on the shape and the mixing efficiency of a free planar jet.

The interest in the effect of periodic disturbances on jets dates back to the mid-1800s when Plateau,[1] in 1857, described the effect of externally applied vibrations to gravitationally induced liquid jets, and LeConte,[2] in 1858, observed the effect of acoustical excitation on gas jets. Since the early 1970s, periodically disturbed jets have been used to study the development of large-scale structures. Most studies were concerned with small-amplitude, high-frequency disturbances applied to axisymmetric jets.[3] Previous research has not addressed the overall characteristics of planar jets under the influence of large-amplitude, low-frequency disturbances.

Description of Test Loop and Procedures

Test Loop

Periodically pulsing the jet upstream of the outlet results in fluctuations of the velocity about some mean velocity. The forced disturbance was caused by periodically restricting the flow, leading to periodic velocity variations. Generally, externally applied disturbances have been small, less than 2% of the mean velocity. However, the amplitudes of the disturbances in this study were, at times, as high as the mean velocity.

The disturbance frequencies examined in this study ranged from 0 Hz, the natural jet, into the audible range to 56 Hz. The subaudible range, below 20 Hz, was of particular interest because of the heating, cooling, and ventilation applications that motivated this study.

In shear flows, naturally occurring and forced frequencies are commonly represented by the Strouhal number,

$$Str = fB/u_0 \tag{1}$$

The Strouhal numbers corresponding to the forced disturbances are shown in Table 1. Exit velocities were on the order of 4 m/s.

The planar jet examined for this study was produced by a slot diffuser 119 cm long by 2.54 cm wide, as shown in Fig. 1. The diffuser was located in a room 5.2 m wide, 10.7 m long, and 2.6 m

Received Feb. 12, 1993; revision received Aug. 9, 1993; accepted for publication Aug. 16, 1993. This paper is declared a work of the U.S. Government and is not subject to copyright protection in the United States.

*Senior Mechanical Engineer, Building and Energy Systems Division, 1617 Cole Boulevard.
†Research Participant, Building and Energy Systems Division, 1617 Cole Boulevard.

Table 1 Disturbance frequencies tested

Disturbance frequency, Hz	Strouhal no.
0	0.000
2	0.011
10	0.057
16	0.090
20	0.112
30	0.168
40	0.230
50	0.290
56	0.324

high. The X, Y, and Z axes represent the axial, transverse, and longitudinal directions, respectively. All dimensions in the flowfield were nondimensionalized by the nozzle width. The diffuser was located about 2.5 m away from the walls and oriented so that the jet issued vertically upward, allowing convenient access to the jet for measurement and flow visualization. The outlet velocity was high enough that the orientation of the nozzle did not affect the jet performance. The Richardson number at the exit, based on the nozzle width and temperature difference between the jet exit temperature and the ambient, was 0.00103, showing that the buoyancy forces were much less than the inertial forces. The nozzle was designed to approximate actual slot diffusers and to have a uniform outlet velocity.

Cold air was supplied to the nozzle via a 20.3-cm-diam galvanized duct by a blower located in an adjacent room along with a chiller. The supply air was 10–20°C cooler than the ambient air. The mechanism used to produce the disturbances was located 4.5 m upstream of the nozzle outlet. The disturbances were generated by rotating a disk perpendicular to the flow inside the duct. When in the fully closed position, twice for each full rotation, the disk occluded the cross-sectional area of the duct by 90%. Screens and turning vanes downstream of the disturbance mechanism insured that turbulent structures produced by the flow over the disk did not reach the outlet.

The natural jet had a Reynolds number

$$Re = u_0 B/\nu \tag{2}$$

of about 7.2×10^3. The increased pressure drop caused by the rotation of the damper decreased the flow rate by about 11%. The flow rate was adjusted to maintain a constant flow rate of 94.4 L/s (200 scfm) at all disturbance frequencies for the images taken from the front view. The flow rate for images taken from the side view was not adjusted.

The shape factor of the boundary layer at the exit, defined as the ratio of the displacement thickness to the momentum thickness, varied from 1.24 for the disturbed jet to 1.78 for the natural jet. This compares with a value of 2.59 for the Blasius profile of a laminar jet. The turbulence intensity at the exit of the natural jet was about 1.5%.

Infrared Imaging Technique

Because air is transparent to infrared radiation, a 70% porous, mesh fiber screen was placed in the flow as a target for the infrared camera. As the chilled air passed over the screen, the screen assumed the temperature distribution of the jet in the plane of the screen and emitted infrared energy.[4] The screen had a response time of about 0.3 s.

The front views are of the $Z \approx 0.5$ plane, and the side views are of the $Y = 0$ plane. Hot-wire anemometry data and images taken of various Z = const planes verified that the $Z \approx 0.5$ plane was free of end effects.

Each infrared image contained more than 68,000 data points and could be updated 30 times per second, providing significantly more information than could be provided by single-point measurements. We used digital averaging of 120 images, one image taken each second for 2 min, to reduce random variations in the temperature distributions. Each image consisted of the average of two frames (1/30th of a second apart).

Nondimensionalizing was used to reduce bias error in measurements. The nondimensional temperature is defined as

$$\Theta(X, Y) = [T(X, Y) - T_{\text{jet}}]/[T_{\text{ambient}} - T_{\text{jet}}] \tag{3}$$

where $T(X, Y)$ is the temperature at any location in the Z = const plane, T_{jet} is the outlet temperature at $(X, Y) = (0, 0)$, and T_{ambient} is the temperature of the surrounding room air. The value of the nondimensional temperature varies from 0 at the nozzle exit to 1 for ambient air.

The full data set contained 68,056 data points. Creating contour plots from this many data points is beyond the capacity of many personal computers. To reduce these data sets to a manageable size for contour plotting, unweighted, nine-point area averaging was used. The averaged data provided a good representation of the full data set.[5]

Figure 2 shows that the transverse velocity profile measured by a constant-temperature, hot-wire anemometer for the isothermal, natural jet is in good agreement with those obtained by Heskestad,[6] Gutmark and Wygnanski,[7] and Sfeir.[8] The curve taken for the present study and the curve taken by Sfeir were taken at $X = 20$, and the other two curves were taken at $X = 65$ (where X is the axial distance nondimensionalized by the nozzle width).

The screen introduces a boundary layer in the flowfield. The roughness of the mesh screen results in a turbulent boundary layer significantly larger than for a smooth surface.[9] The screen, when viewed from the front of the jet, cuts across the jet and does not produce what is ordinarily considered a wall jet. The roughness of the screen increases the Nusselt number[10] because large velocity fluctuations in the boundary layer transport mass and energy from the freestream flow to the screen, keeping the temperature of the

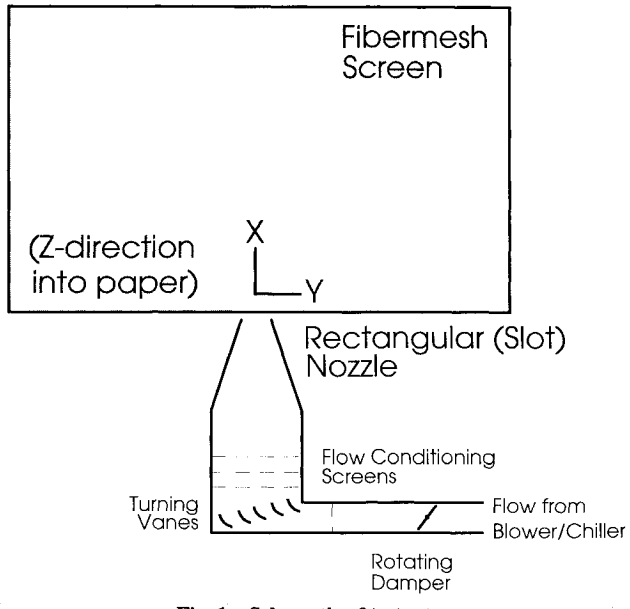

Fig. 1 Schematic of test setup.

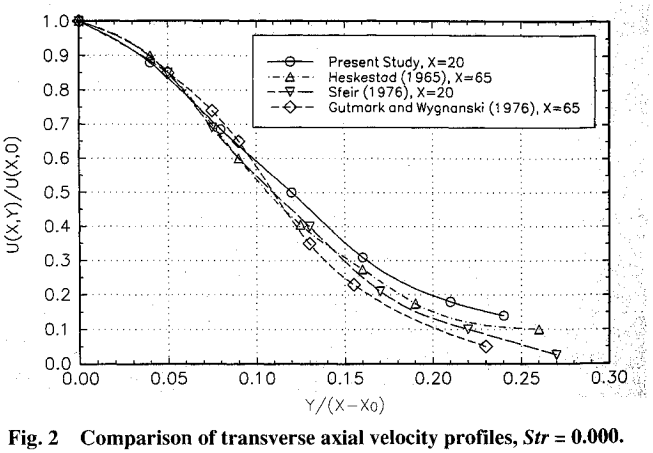

Fig. 2 Comparison of transverse axial velocity profiles, *Str* = 0.000.

screen in equilibrium with the freestream flow. Preliminary measurements with thermocouples indicate a uniform temperature within the velocity boundary layer.

High-Speed Flow Visualization

The infrared imaging system provides a comprehensive but averaged representation of the temperature field of the pulsed jet. To get an instantaneous view of the effect of the disturbances on the vortical fluid structures by which mixing occurs, we took photographs of smoke-wire flow visualization at a shutter speed of 1/6400 s. This was a sufficiently small time span to observe the development and interaction of individual fluid structures.

Test Results

Self-Similar Transverse Profiles

The transverse temperature profiles for the natural jet at various axial distances are shown in Fig. 3a. In the region near the exit, the jet is developing and has not yet assumed the self-similar temperature profiles found in the fully developed region. The profiles are self-similar by 9.2 nozzle widths from the exit and follow a Gaussian distribution. The transverse temperature profile nondimensionalized by the temperature half-width are shown in Figs. 3b and 3c for axial distances of 4.9 and 20.2 along with a Gaussian profile. The results indicate that the effect of the mesh fiber screen on the development of the temperature field of the jet is negligible within the region studied.[5]

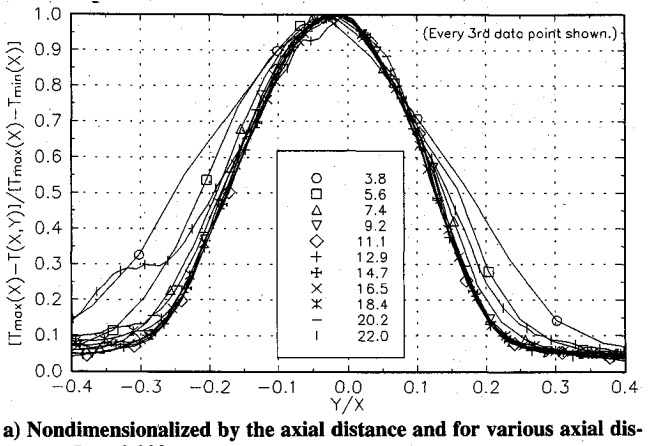

a) Nondimensionalized by the axial distance and for various axial distances, *Str* = 0.000

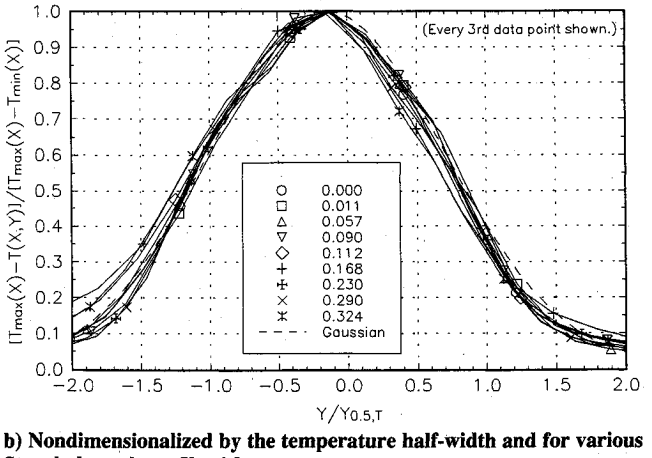

b) Nondimensionalized by the temperature half-width and for various Strouhal numbers, *X* = 4.9

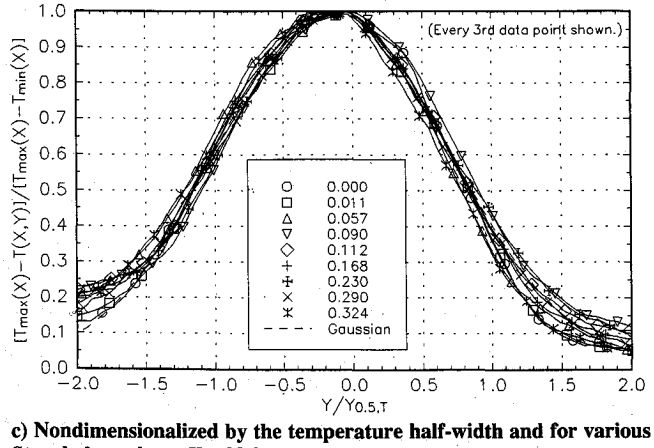

c) Nondimensionalized by the temperature half-width and for various Strouhal numbers, *X* = 20.2

Fig. 3 Transverse temperature profiles.

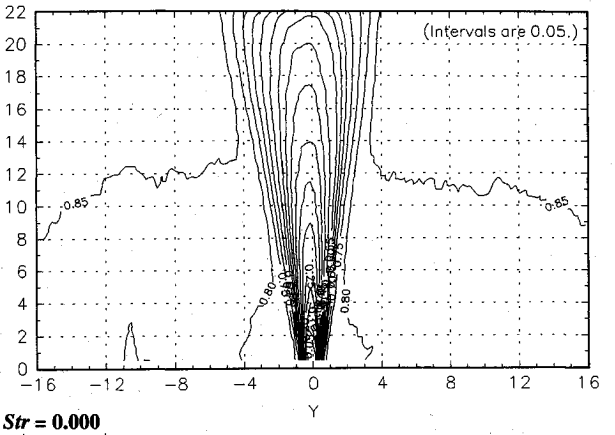

a) *Str* = 0.000

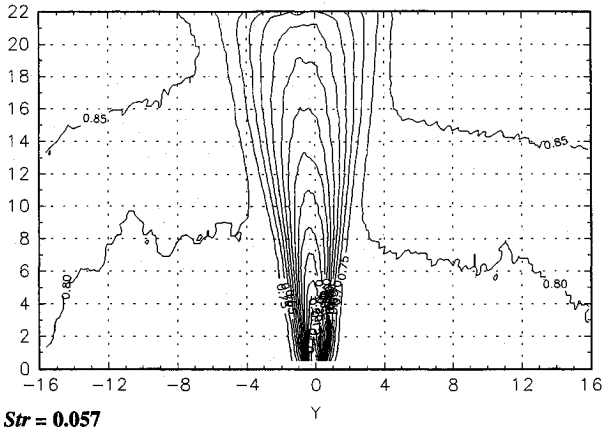

b) *Str* = 0.057

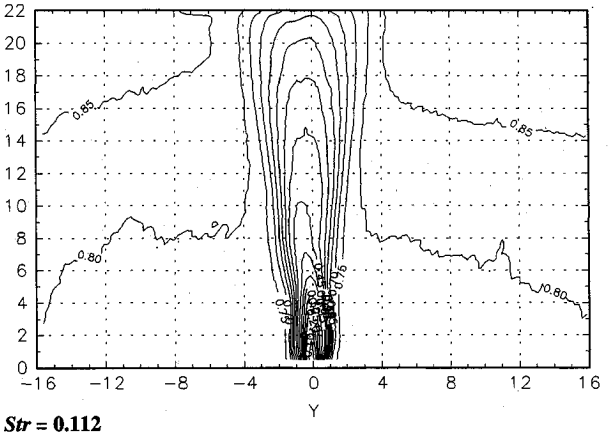

c) *Str* = 0.112

Fig. 4 Transverse isotherms from infrared images.

Contour Plots

Isotherms of front view infrared images for the jet disturbed at Strouhal numbers of 0.000, 0.057, and 0.112 are shown in Fig. 4. The jet boundaries of the undisturbed jet, shown in Fig. 4a, are nearly vertical throughout the first nozzle width of axial distance. The transverse temperature gradient is steep. The contour for the 0.50 isotherm extends to 20 nozzle widths, indicating the throw of air that is midpoint in temperature between T_{jet} and $T_{ambient}$.

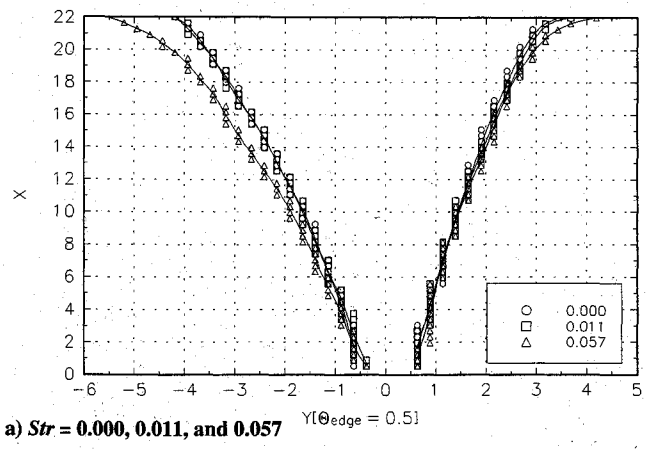

a) ***Str* = 0.000, 0.011, and 0.057**

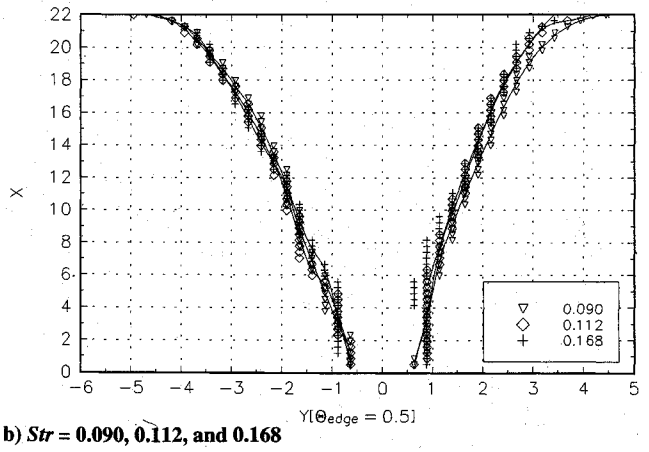

b) ***Str* = 0.090, 0.112, and 0.168**

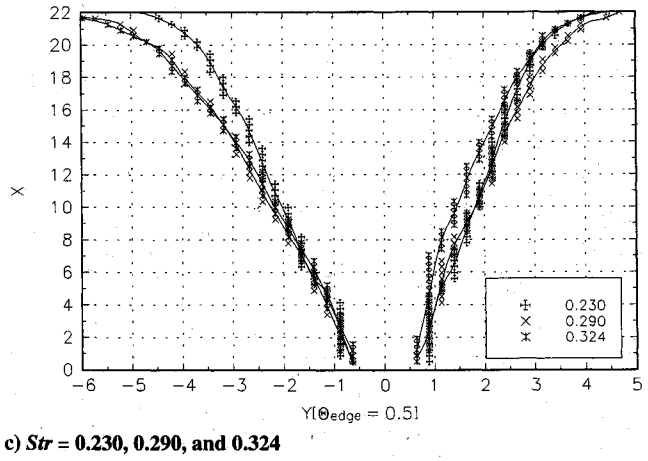

c) ***Str* = 0.230, 0.290, and 0.324**

Fig. 5 Jet half-width.

The effect of disturbance of the jet at $Str = 0.057$ is shown in Fig. 4b. The width of the jet, caused by greater spreading, is much greater over the first nozzle width. The transverse temperature gradient is not as steep, and the 0.50 isotherm now extends only to 16 nozzle widths or about 75% of the distance of the natural jet.

A greater effect can be seen in Fig. 4c when the jet is disturbed at $Str = 0.112$. The jet has a greater spread angle near the nozzle exit, reducing the slope of the transverse temperature gradient even further. The peak of the 0.50 isotherm is now only about 14 nozzle widths or about 70% of the distance of the natural jet. The disturbances on the jet increased the spread of the jet and decreased the throw of the jet.

Jet Half-Widths

The change in the spread rate of the jet can be measured by inspection of the infrared images. The jet thermal half-width is defined as the transverse point at a given axial distance where the difference between the temperature at that point and the minimum temperature is one-half the difference between the ambient temperature and the minimum jet temperature,

$$Y_{0.5} = Y\left[\frac{T(X,Y) - T_{\min}(X)}{T_{\max}(X) - T_{\min}(X)} = 0.5\right] \tag{4}$$

The location of the half-width, $Y_{0.5}$, is where the jet edge nondimensional temperature, or Θ_{edge}, is equal to 0.5. The variable Θ_{edge} may be chosen as any value of the ratio in Eq. 4.

The jet half-width for different Strouhal numbers, given in Fig. 5, increases with increasing disturbance frequency. Disturbances at Strouhal numbers of 0.112, 0.168, and 0.230 have the greatest effect near the nozzle exit. At Strouhal numbers higher than 0.230, the greatest spreading occurs farther downstream. It is important to note that Θ_{edge} represents a ratio of temperature differences and not the actual temperature of the jet edge. Because the centerline temperature warms more quickly for the disturbed jets, the actual temperature at a particular Θ_{edge} will be greater than that for the undisturbed jet. Therefore, the contour plots show greater spreading of

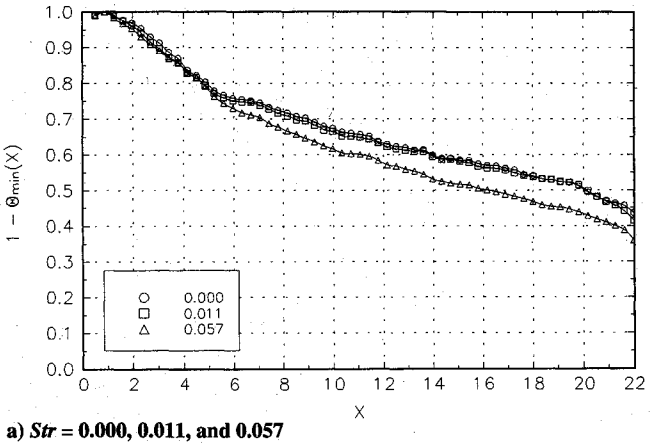

a) ***Str* = 0.000, 0.011, and 0.057**

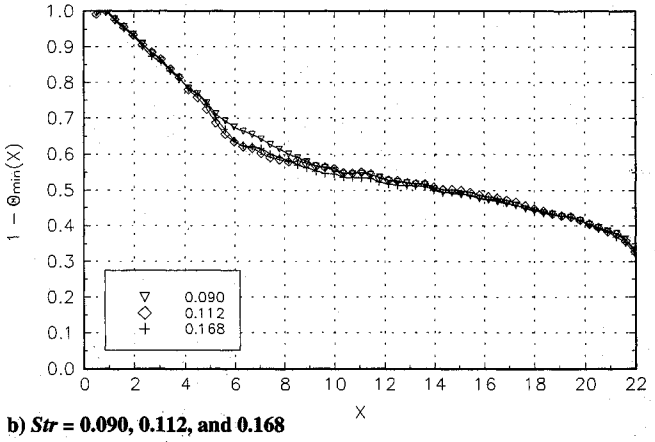

b) ***Str* = 0.090, 0.112, and 0.168**

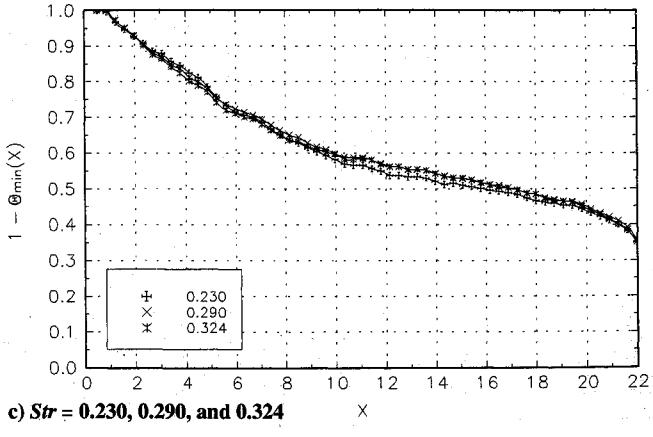

c) ***Str* = 0.230, 0.290, and 0.324**

Fig. 6 Axial temperature decay.

the jet near the nozzle exit than is apparent from the plots of the jet half-widths.

Jet Centerline Temperature

The jet centerline is represented by the coolest part of the jet, the jet minimum temperature. As the cool jet mixes with the surrounding air, the temperature of the jet increases. The rate of axial decay of the temperature indicates how quickly ambient air is reaching the coolest part of the jet. A plot of the axial decay of temperature to the ambient temperature is shown in Fig. 6. The temperature decay is greatest at Strouhal numbers of 0.112 and 0.168, but any disturbance at or above $Str = 0.057$ has a significant effect on the temperature decay.

A notable feature in Fig. 6 is the two distinct regions on the curves over which they are nearly linear. The slope of the curves for the natural jet and the pulsed jet changes sharply at about six nozzle widths downstream. The change in slope of the curves of the jet pulsed at Strouhal numbers greater than 0.168 is more gradual than the change for those of Strouhal numbers at and below 0.168.

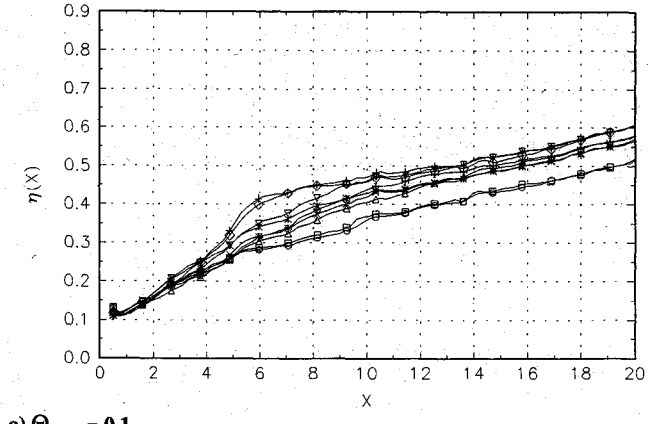

a) $\Theta_{edge} = 0.1$

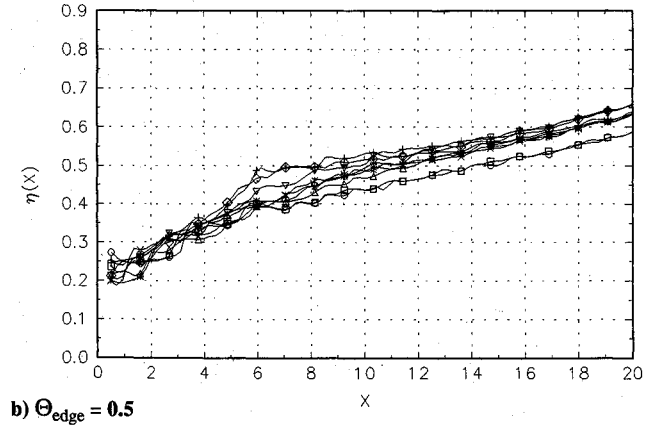

b) $\Theta_{edge} = 0.5$

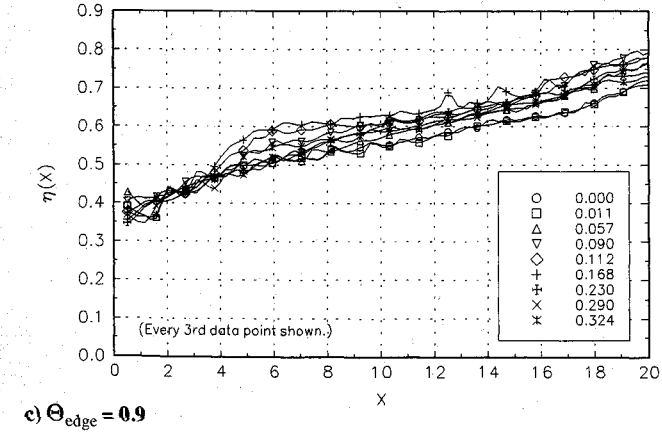

c) $\Theta_{edge} = 0.9$

Fig. 7 Mixing efficiency vs axial distance for various Strouhal numbers.

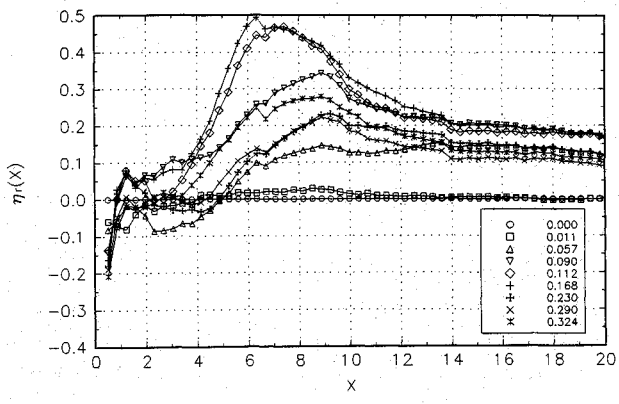

a) $\Theta_{edge} = 0.1$

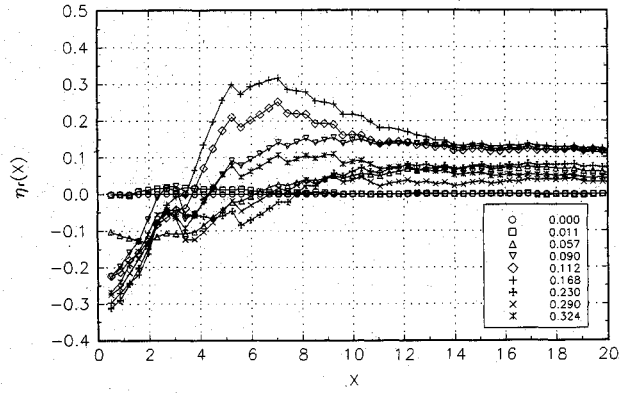

b) $\Theta_{edge} = 0.5$

Fig. 8 Relative mixing efficiency vs axial distance for various Strouhal numbers.

Jet Mixing Efficiency

Entrainment is a measure of the amount of ambient air brought into the jet. This is normally shown as an increase in the mass of the jet and requires a knowledge of the velocity distribution. Because this information is not directly available from the infrared images, the mass flow entrainment will be related to the temperature distribution by a thermal mixing efficiency. We defined a thermal mixing efficiency as the integral of nondimensional temperature between the jet edges,

$$\eta(X) = \frac{1}{(Y^+ - Y^-)} \int_{Y^-}^{Y^+} \Theta(X, Y)\, dY \tag{5}$$

Because temperature is a scalar, it can be used as a passive tracer to determine mixing in the jet. The Y^+ and Y^- represent the jet edges, Θ_{edge}, in the positive and negative transverse directions, respectively. The value of the mixing efficiency is 0 when the temperature profile between the jet edges is uniform at the jet minimum temperature, indicating that no mixing has occurred. The mixing efficiency equals 1 when the temperature profile is uniform at the ambient room air temperature, indicating that complete mixing has occurred. The mixing efficiency is the average nondimensional temperature at a particular axial distance and represents the mixing of the jet that has occurred from the exit to X.

The mixing efficiencies are given in Fig. 7 for three values of the jet-edge temperature. The mixing efficiency of the jet disturbed at $Str = 0.112$, with $\Theta_{edge} = 0.5$, and at six nozzle widths, is 19% greater than that for the natural jet. The disturbance causes significantly increased mixing in the core of the jet by six nozzle widths as demonstrated by Fig. 7a.

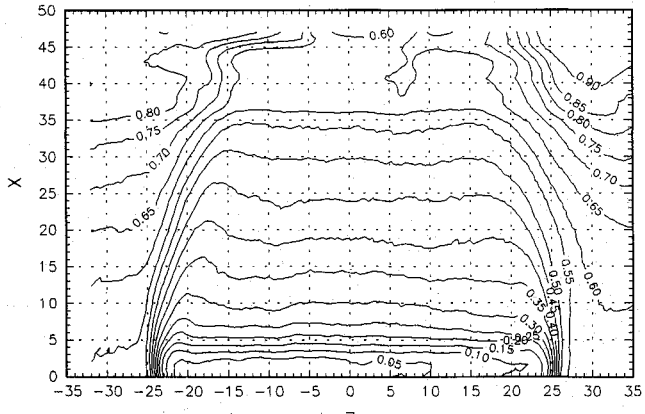

a) *Str* = 0.000 and 94.4 L/s

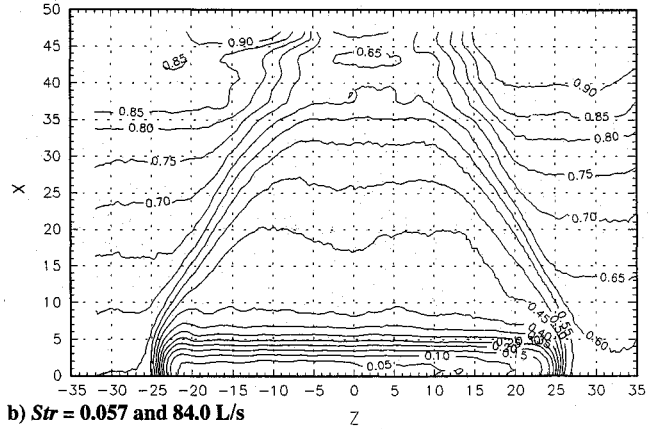

b) *Str* = 0.057 and 84.0 L/s

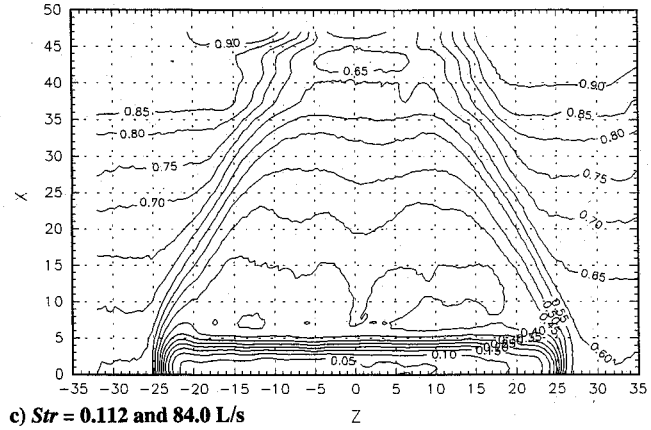

c) *Str* = 0.112 and 84.0 L/s

Fig. 9 Longitudinal isotherms from infrared images.

The mixing efficiency curves for the jet pulsed at $Str = 0.112$ are nearly linear over two distinct regions, corresponding to the same regions of linearity on the curves of axial temperature decay.

Relative Mixing Efficiency

To give a direct comparison of the mixing efficiency of the pulsed jet to that of the natural jet, we defined a relative mixing efficiency as

$$\eta_r(X,f) = \frac{\int_{Y^-(f=0)}^{Y^+(f=0)} \Theta(X,Y,f)\,dY - \int_{Y^-(f=0)}^{Y^+(f=0)} \Theta(X,Y,0)\,dY}{\int_{Y^-(f=0)}^{Y^+(f=0)} \Theta(X,Y,0)\,dY} \tag{6}$$

The nondimensional temperatures are integrated between the edges of the natural jet. The relative mixing efficiency compares the degree of mixing that has occurred within the same physical area for the disturbed and natural jets. Figure 8 shows the relative mixing efficiencies of several disturbance frequencies at $\Theta_{edge} = 0.1$ and 0.5. Mixing in the very core of the jet, where $\Theta_{edge} = 0.1$, is nearly 50% greater than that of the natural jet at six nozzle widths, for $Str = 0.168$. The mixing of the jet pulsed at $Str = 0.168$ that occurs within the half-width, $\Theta_{edge} = 0.5$, of the natural jet is about 32% greater at seven nozzle widths than that of the natural jet.

The relative mixing efficiencies for Strouhal numbers greater than 0.011 are negative below about four nozzle widths because of the definition of the jet edge. The jet boundaries for the limits of integration in Eq.(6) are determined by the shape of the natural jet, which has a narrower spread angle than the pulsed jet. Because the pulsed jet has a much greater spread angle over the first few nozzle widths, Eq. (6) is integrated over only a portion of its cross section for axial positions in this region. The cold core of the pulsed jet extends beyond the location of the warmer edge of the natural jet near the nozzle exit. The relative mixing efficiency is a measure of how much the disturbed jet has warmed by a given axial distance compared with the natural jet; both are evaluated only within the region defined by the edges of the natural jet.

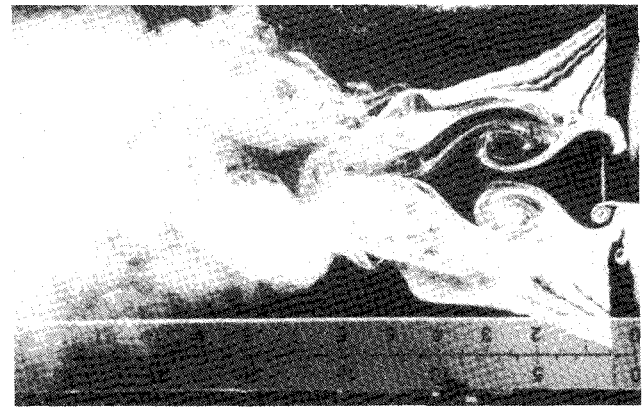

a) *Str* = 0.000

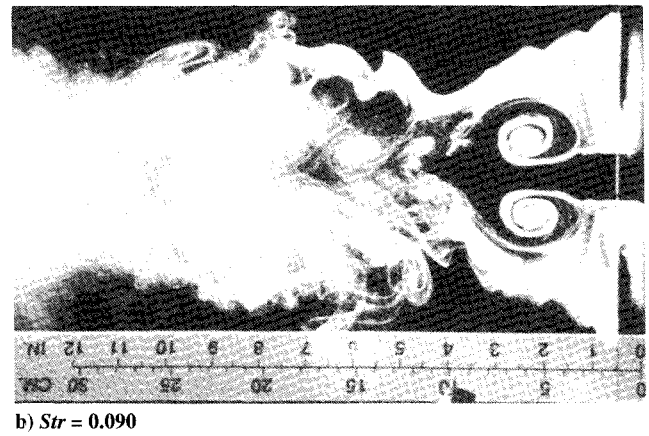

b) *Str* = 0.090

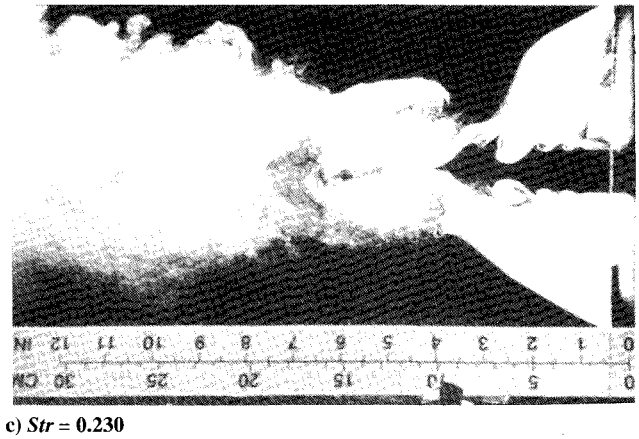

c) *Str* = 0.230

Fig. 10 High-speed smoke-wire visualization.

Side View

The entrainment of ambient air up to a given axial distance in a planar jet is proportional to the square root of the distance. In an axisymmetric jet, the entrainment is directly proportional to the axial distance.[11] Therefore, an early transition of a planar jet into an axisymmetric jet will enhance entrainment. An early transition requires that the increased spreading seen in the front view be accompanied by the drawing in of the jet ends in the longitudinal direction. The side view images reveal the effect of the disturbances on the transition of the planar jet into the axisymmetric regime.

Isotherms from infrared images of the side view of the jet are shown in Fig. 9 for the jet pulsed at Strouhal numbers of 0.000, 0.057, and 0.112. The longitudinal temperature profiles show a dip in the center of the profile with peaks toward either end. This is the saddle-back shape identified by van der Hegge Zijnen[12] for velocity and temperature profiles. The images taken from the side view were at a flow rate of 94.4 L/s for the undisturbed case. The flow was not adjusted to account for reduced flow when the disturbances were generated. Therefore, at $Str = 0.112$, the flow rate was 84 L/s (178 scfm). Other tests showed that the shape of the temperature profile was not sensitive to the flow rate.

Disturbing the jet draws in the ends of the jet and causes the peaks of the saddle-back shape to move closer to the longitudinal center of the jet. The reduction of the throw of cold air can be seen. The disturbed jet will become axisymmetric closer upstream, nearer the nozzle exit, than will the natural planar jet. The disturbance accelerates the transition to an axisymmetric regime.

High-Speed Smoke-Wire Visualization

High-speed photographs of smoke-wire flow visualization, shown in Fig. 10, give insight into the structural phenomena that produce the overall behavior seen from the infrared images. Figure 10a shows the structures found in the natural jet. The vortical structures at the jet boundaries are small and may be either symmetric or antisymmetric. The jet boundaries are nearly vertical for the first nozzle width of the jet.

When the jet is disturbed, the velocity fluctuates periodically, and large, symmetrical pairs of vortices are formed near the outlet. These large, periodic, symmetric vortices do not form in the natural jet and are a result of the disturbances. Figure 10c shows a symmetric vortex pair, in the early stages of its development, that is responsible for the bulging of the jet near the outlet, as seen by the infrared imaging. The axial distance where these structures coalesce, $X = 6$ to $X = 8$, coincides with the sudden changes of slope in the curves of axial velocity decay and mixing efficiency.

Concluding Remarks

Large-amplitude, low-frequency periodic disturbances, corresponding to Strouhal numbers from 0.000 to 0.324, have a significant effect on the shape and the decay characteristics of a free planar jet. In general, large-amplitude disturbances increase the angle of spread of the jet in the X-Y plane and shorten the inviscid core. This decreases the throw of the jet. The axial temperature decay is accelerated, and the mixing efficiency of the jet is increased. The relative mixing efficiency is increased more by disturbance at $Str = 0.168$ than for any other disturbance frequency observed. The mixing of the jet with its surroundings is a result of the natural instabilities of the jet. The periodic disturbances enhance these instabilities, resulting in increased mixing. Moore[13] observed that, although low-level acoustical excitation produced a response in agreement with linear stability theory, high-level acoustical excitation led to nonlinear response and changed the jet turbulent structure. Large-amplitude forcing, as reported here, leads to temporal, as well as spatial, velocity gradients in the shear layer. These velocity gradients enhance the natural instability of the jet, leading to early vortex generation. The early vortex generation is responsible for the wider spread angle of the forced jet.

The natural jet entrains mass and mixes with the surrounding air, in part, through the formation and breakdown of vortical structures. However, the structures found in the natural jet are smaller and less ordered than those found in the pulsed jet. The formation of large, periodic vortices by large-amplitude disturbances increases mixing and spreading of the jet. The instantaneous boundaries of the jet during pulsing fluctuate in and out as these vortices form, grow, and are carried downstream. However, the fluctuations of the jet boundaries are time averaged by the imaging technique employed for this study. The time-averaged boundaries of the disturbed jet, as shown by infrared imaging, are wider than the natural jet.

Disturbing the jet draws in the ends of the jet in the longitudinal direction, accelerating the transition to an axisymmetric regime. The peaks of the saddle-back shape, seen in the longitudinal temperature profiles, move toward the middle of the jet as a result of disturbing the jet.

The results presented in this paper demonstrate the advantages of using digital imaging analysis as a means of gaining quantitative information from a plane of a flowfield. Obtaining the equivalent information using point measurements would be impractical and intrusive to the flow. The results using this technique provide rapid and comprehensive information about the temperature distribution and thermal mixing in the flowfield.

References

[1]Plateau, J., "Experimental and Theoretical Researches on the Figures of Equilibrium of a Liquid Mass Withdrawn from the Action of Gravity—Theory of the Modifications Experienced by Jets of Liquid Issuing from Circular Orifices When Exposed to the Influence of Vibratory Motions," *The London, Edinburgh and Dublin Philosophical Magazine and Journal of Science*, 4th Series, Vol. XIV, 1857, pp. 1–22.

[2]LeConte, J., "On the Influence of Musical Sounds on the Flame of a Jet of Coal-Gas," *The London, Edinburgh and Dublin Philosophical Magazine and Journal of Science*, 4th series, Vol. XV, 1858, pp. 235–239.

[3]Hussain, A. K. M. F., and Zaman, K. B. M. Q., "The 'Preferred Mode' of the Axisymmetric Jet," *Journal of Fluid Mechanics*, Vol. 110, 1981, pp. 39–71.

[4]Anderson, R., Hassani, V., Kirkpatrick, A., Knappmiller, K., and Hittle, D., "Visualizing the Air Flow from Cold Air Ceiling Jets," *American Society of Heating, Refrigerating, and Air-Conditioning Engineers Journal*, May 1991, pp. 30–35.

[5]Farrington, R., "The Effect of Large-Amplitude, Low-Frequency Excitation on a Three Dimensional Jet," Ph.D. Thesis, Dept. of Mechanical Engineering, Univ. of Colorado, Boulder, CO, 1992, pp. 400, 717.

[6]Heskestad, G., "Hot-Wire Measurements in a Plane Turbulent Jet," *Journal of Applied Mechanics*, Transactions of the American Society of Mechanical Engineers, Vol. 32, Dec. 1965, pp. 721–734.

[7]Gutmark, E., and Wygnanski, I., "The Planar Turbulent Jet," *Journal of Fluid Mechanics*, Vol. 73, Pt. 3, 1976, pp. 465–495.

[8]Sfeir, A. A., "The Velocity and Temperature Fields of Rectangular Jets," *International Journal of Heat and Mass Transfer*, Vol. 19, 1976, pp. 1289–1297.

[9]Clauser, F. H., "The Turbulent Boundary Layer," *Advances in Applied Mechanics*, Vol. 4., No. 1, 1956, p. 4.

[10]Cebeci, T., and Bradshaw, P., *Physical and Computational Aspects of Convective Heat Transfer*, Springer-Verlag, New York, 1984, pp. 225, 226.

[11]Rajaratnam, N., *Turbulent Jets*, Elsevier Scientific, Amsterdam, The Netherlands, 1976, pp. 25, 36.

[12]van der Hegge Zijnen, B. G., "Measurements of the Distribution of Heat and Matter in a Plane Turbulent Jet of Air," *Applied Scientific Research*, Sec. A, Vol. VII, 1958, pp. 277–292.

[13]Moore, C. J., "The Role of Shear-Layer Instability Waves in Jet Exhaust Noise," *Journal of Fluid Mechanics*, Vol. 80, Pt. 2, 1977, pp. 322–367.